RSC Advances

PAPER

View Article Online
View Journal | View Issue

Cite this: *RSC Adv.*, 2014, **4**, 44175

Highly-efficient steam reforming of methanol over copper modified molybdenum carbide

Yufei Ma,[a] Guoqing Guan,*[ab] Xiaogang Hao,[c] Zhijun Zuo,[c] Wei Huang,[c] Patchiya Phanthong,[a] Katsuki Kusakabe[d] and Abuliti Abudula*[ab]

Received 13th June 2014
Accepted 5th September 2014

DOI: 10.1039/c4ra05673f

www.rsc.org/advances

Cu doped molybdenum carbide (Cu–Mo_xC_y) catalysts were prepared by carburization of Cu doped molybdenum oxide (Cu–MoO_3) using a temperature-programmed reaction with a 20% CH_4–H_2 mixture at 700 °C. Phase transition of the prepared molybdenum carbide was found to be related to the doping amount of Cu: with the increase in the doping amount of Cu/Mo molar ratio of 1.6/98.4 to 10/90, the cubic α-MoC_{1-x} phase increased in the catalyst, but with the continued increase of the doping amount to a Cu/Mo molar ratio of 15/85, the α-MoC_{1-x} phase began to decrease, and when the Cu doping amount reached a Cu/Mo molar ratio of 25/75, the α-MoC_{1-x} phase became very weak and mainly hexagonal β-Mo_2C phase was found in the catalysts. TEM images indicated that carbon growth on the surface of Cu occurred during the carburization process in the case of high Cu doping. Steam reforming of methanol (SRM) over the Cu–Mo_xC_y catalyst was investigated at a temperature range of 200–400 °C. It is found that Cu–Mo_xC_y catalyst with Cu/Mo molar ratios in the range of 1.6/98.4–10/90 showed high catalytic activity as well as long-term stability. X-ray photoelectron spectroscopy analysis indicated the coexistence of Cu^{I} and Cu^{II} species on the surface of the molybdenum carbide. The existence of Cu^{I} could result in high activity for methanol conversion and high stability, which might result from the strong interaction between Cu and Mo_2C support.

Introduction

Molybdenum carbide (Mo_2C) is attractive due to its noble-metal-like catalytic activity for many important reactions such as NH_3 synthesis,[1] water gas shift (WGS),[2–4] methane dry reforming[5] and decomposition or steam reforming of methanol.[6–9] To prepare Mo_2C based catalysts, the temperature-programmed reaction (TPRe) method, in which the solid-state transformation of molybdenum oxide (MoO_3) in a controlled manner by reacting MoO_3 with carbon-containing gas mixtures such as CH_4–H_2[10–12] and C_2H_6–H_2,[13] has been developed. It is found that loading of other metals on MoO_3 can reduce the temperature for MoO_3 reduction and increase the specific surface area of the produced carbide.[14] The molybdenum carbide phase can also be altered by loading of different transition metals: Pt, Pd or Ni loading always produces the cubic α-MoC_{1-x} phase while Co or Cu loading could result in the hexagonal β-Mo_2C phase, which is the same phase as that produced from direct transformation of MoO_3 itself without any metal loading.[14] In our previous studies,[6,15,16] various transition metals such as Pt, Fe, Co, and Ni were doped on the molybdenum carbide, and found that the β-Mo_2C phase was formed by doping Fe, Co, or Ni while α-MoC_{1-x} phase was appeared with the β-Mo_2C phase in the case of Pt doping. Especially, with the increase in Pt doping amount, more α-MoC_{1-x} phase was produced, indicating that the loading amount had great effect on the obtained phase of molybdenum carbide.

Steam reforming of methanol (SRM) is considered a promising way for the on-board H_2 production.[17,18] SRM has been performed over various catalysts, including noble and non-noble metal catalysts,[19–22] in which Cu-based catalysts are preferred due to its high catalytic activity and low cost. In recent years, molybdenum carbide and transition metal doped molybdenum carbide were also developed for the SRM reaction.[6–9] However, to date, Cu doped molybdenum carbides are seldom investigated.[14] If Cu is combined with molybdenum carbide, it is possible to obtain a new series of catalyst for the SRM reaction. Based on this consideration, in the present study, Cu doped molybdenum carbides with different Cu loading amounts were prepared by carburization of Cu-doped MoO_3 in a gas mixture of 20% CH_4–H_2, and applied for the SRM reaction at different temperatures. The morphologies, crystal phase transitions, surface areas and surface species states were

[a]*Graduate School of Science and Technology, Hirosaki University, 3 Bunkyo-cho, Hirosaki, Aomori 036-8561, Japan*

[b]*North Japan Research Institute for Sustainable Energy, Hirosaki University, 2-1-3 Matsubara, Aomori 030-0813, Japan. E-mail: guan@cc.hirosaki-u.ac.jp; abuliti@cc.hirosaki-u.ac.jp; Fax: +81 17 735 5411; Tel: +81 17 762 7756*

[c]*Department of Chemical Engineering, Taiyuan University of Technology, Taiyuan 030024, China*

[d]*Department of Nanoscience, Sojo University, 4-22-1 Ikeda, Kumamoto 860-0082, Japan*

characterized using SEM, TEM, XRD, BET and XPS respectively with an endeavor to understand the relationship between the catalytic activity and the microstructure and physicochemical property of Cu-doped molybdenum carbide.

Experimental

Catalyst preparation

Oxide precursors (Cu–MoO_3) of Cu doped molybdenum carbides with different Cu/Mo initial molar ratios of 1.6/98.4, 5/95, 10/90, 15/85 and 25/75 were prepared using mixtures of aqueous solutions of copper nitrate ($Cu(NO_3)_2 \cdot 3H_2O$; Sigma-Aldrich Co., 99%) and ammonium heptamolybdate ($(NH_4)_6Mo_7O_{24} \cdot 4H_2O$; Kojundo Chemical Laboratory Co., 99%). The chemicals were dissolved in distilled water at 25 °C under stirring for 4 h at first, which produced a viscous mixture, and then the mixture solution was continuously stirred in oil bath at 80 °C until dried. After the solid product was dried at 110 °C overnight, it was calcined in air at 500 °C for 4 h. Carburization of the as-prepared Cu–MoO_3 was carried out in a fixed-bed quartz micro-reactor with an inner diameter of 10 mm, in which Cu–MoO_3 powder was placed on a porous quartz plate, and then carburized in CH_4–H_2 (20 vol% CH_4) atmosphere with a successive temperature-programmed process: the carburization temperature was raised from the room temperature (RT) to 300 °C at a rate of 5 °C min^{-1}, and then increased to 700 °C at a rate of 1 °C min^{-1}, and finally kept at 700 °C for 2 h. Thereafter, the reactor was cooled down to RT in CH_4–H_2 flow and then the product was passivated in 1%O_2/Ar for 12 h at RT. For comparison, MoO_3 powder was also prepared by calcination of $(NH_4)_6Mo_7O_{24} \cdot 4H_2O$ at 500 °C for 4 h in air and then carburized using the same method. In the present study, the as-prepared Cu–Mo_xC_y catalysts with different Cu/Mo initial molar ratios of 1.6/98.4, 5/95, 10/90, 15/85, 25/75 were denoted hereinafter as Cu–Mo_xC_y (1.6), Cu–Mo_xC_y (5), Cu–Mo_xC_y (10), Cu–Mo_xC_y (15), Cu–Mo_xC_y (25), respectively.

Catalyst characterization

Crystal structures of the catalysts before and after the reaction were determined by X-ray diffraction (XRD 610, Shimadzu, Japan). The radiation used was Cu Kα and the operating potential was 30 kV, current 30 mA, and the scanning rate 4° min^{-1}; phase identification was achieved through comparison of XRD patterns to those of "Joint Committee on Powder Diffraction Standards (JCPDS)". BET (Brunauer–Emmett–Teller) surface areas were measured through nitrogen adsorption at 77 K using a Quantachrome NOVA 4200e Surface Area and Pore Size Analyzer. The microstructure and morphology were characterized with a scanning electron microscope (SEM, S-800, Hitachi, Japan). Transmission electron microscope (TEM) images were obtained using a JEM-2100F transmission electron microscope JEOL operating at 200 kV. X-ray photoelectron spectroscopy (XPS) analysis was done with AXIS ULTRA DLD spectrometer using Al Kα radiation ($h\nu$ = 1486.6 eV) as the photon source, generation at 150 W. The binding energies of Mo 3d and Cu 2p were analyzed using the Shirley baseline correction.

Catalyst performance evaluation

Catalytic performances of the pure β-Mo_2C and Cu–Mo_xC_y were evaluated in a micro-reactor with an inner diameter of 6 mm. Prior to the reaction, the catalyst was pretreated with 15% CH_4/H_2 at 590 °C for 2 h in order to reduce the oxide on the surface. The pretreatment temperature was chosen based on our preliminary experiments. The total amount of the catalyst used was 0.4 g, and a weight hourly space velocity (WHSV) of 9000 $cm^3\ g^{-1}\ h^{-1}$ was selected in this study. Methanol and water mixture with a molar ratio of 1 : 1 (13% CH_3OH–13% H_2O in Ar) was injected into the reactor with a syringe pump. It was vaporized in a pre-heater containing ZrO_2 beads and carried by Ar gas flow. Catalytic performance was tested at different temperature from 200–400 °C and atmospheric pressure. The sampling was started after 1 hour stabilization at each temperature. Herein, a thermocouple was inserted in the catalytic bed for the reaction temperature control. A water-ice cold trap was set at the exit of the reactor to remove out the unconverted methanol and steam. The products were analyzed using a gas chromatograph with TCD detector (Agilent 7890A GC system) and a gas chromatograph with FID detector (Shimadzu GC-2014). The outlet gas flow rate was determining by inner standard method, in which the flow rates of CH_4, CO, and CO_2 were calculated based on the flow rate of inert gas N_2 in the reaction system while that of H_2 was calculated based on the flow rate of inert gas He in the reaction system.

Performances of the catalysts were characterized in terms of methanol conversion, hydrogen production rate (μmol g-cat^{-1} min^{-1}). The methanol conversion was defined as the molar ratio of the gaseous carbon compounds (CH_4, CO, and CO_2) in the product stream to the feed methanol since only traces of other products such as C_2H_6, C_2H_4 and HCOOH in outlet gas and liquid were detected in this study. Methanol conversion was defined as the followings:

$$X_{CH_3OH} = \frac{n_{CO} + n_{CO_2} + n_{CH_4}}{n_{CH_3OH}} \times 100\% \quad (1)$$

where n_{CO}, n_{CO_2}, n_{CH_4}, and n_{CH_3OH} are the flow rates of CO, CO_2, CH_4 in the outlet reformate and methanol in the feed, respectively. The mole fraction of a product component was defined as the molar ratio of this specific product to the total gaseous product.

Results and discussion

Physicochemical properties of the catalysts

Fig. 1 shows XRD patterns of the as-prepared fresh Cu–Mo_xC_y (Cu/Mo initial molar ratios = 1.6/98.4, 5/95, 10/90, 15/85, 25/75) catalysts. The peaks at 2θ of 34.8°, 38.4° and 39.8° are attributed to the presence of hexagonal β-Mo_2C phase with hcp crystal structure while the peaks at 2θ of 37.1° and 42.8° are attributed to cubic α-MoC_{1-x} phase with fcc crystal structure. The typical peaks corresponding to MoO_3 are those at 2θ of 12.7°, 25.6° and

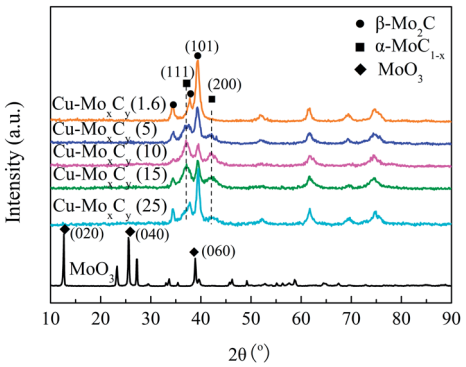

Fig. 1 XRD patterns of Cu doped molybdenum carbide with different doping amounts and MoO_3.

38.9°. For all the as-prepared Cu–Mo_xC_y catalysts, no peaks corresponding to metallic Mo as well as Cu were observed in the present study. As shown in Fig. 1, when the doping amount of Cu with Cu/Mo initial molar ratios of 1.6/98.4, only β-Mo_2C phase was formed in the final catalysts. However, when the Cu/Mo initial molar ratio was 5/95, α-MoC_{1-x} phase began to appear together with the β-Mo_2C phase, and the peaks corresponding to α-MoC_{1-x} phase became more and more obvious with the increase in Cu doping amount, suggesting that more α-MoC_{1-x} phase was produced in the final catalyst, especially for the Cu–Mo_xC_y (10) sample. However, when the Cu/Mo initial molar ratio was increased over 15/85, the strength of the peaks corresponding to α-MoC_{1-x} phase began to decrease, and when the Cu/Mo initial molar ratio reached 25/75, all peaks of α-MoC_{1-x} phase became very weak. In general, thermodynamically metastable fcc α-MoC_{1-x} catalysts with high specific surface area are obtained by TPRe of MoO_3 with ammonia, in which nitride (fcc γ-Mo_2N) was formed at first and subsequently converted to α-MoC_{1-x} phase under methane containing atmosphere.[12–14] It is suggested that the reactions involved in the above both processes are topotactic solid transformation process with the formation of metastable α-MoC_{1-x} crystal, which exhibits the pseudomorphism with the original platelet morphology of MoO_3.[12] In contrast, the hcp structure β-Mo_2C phase was considered to be due to the transformation of MoO_3 to carbide followed a non-topotactic route involving the MoO_2 as the main intermediate,[14] and in this case, the morphology of obtained carbide is also different from the original morphology of MoO_3.

SEM images of MoO_3, β-Mo_2C, Cu–Mo_xC_y (1.6), Cu–Mo_xC_y (5), Cu–Mo_xC_y (10) and Cu–Mo_xC_y (25) are shown in Fig. 2. One can see that the morphology of MoO_3 was platelet-like (Fig. 2(a)) but after the carburization, the morphology of β-Mo_2C (Fig. 2(b)) was changed: many large platelet particles in the original MoO_3 seemed to be broken into smaller ones and numerous agglomerates of small particles were observed, indicating that the non-topotactic transformation occurred during the carburization process. For the Cu–Mo_xC_y with lower Cu loading amount, for instance, Cu–Mo_xC_y (1.6) (Fig. 2(c)), its morphology was almost the same as that of pure β-Mo_2C. However, with the increase in Cu doping amount, for instance,

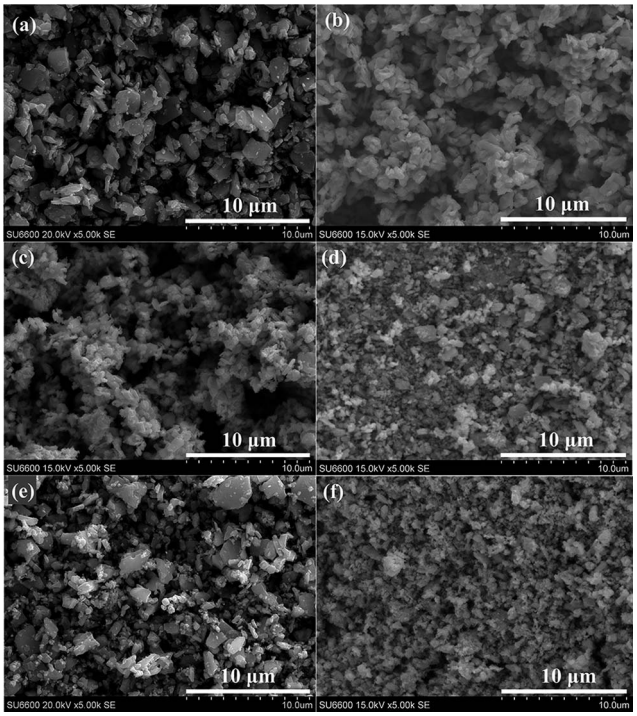

Fig. 2 SEM morphologies of (a) MoO_3, (b) β-Mo_2C, (c) Cu–Mo_xC_y (1.6), (d) Cu–Mo_xC_y (5), (e) Cu–Mo_xC_y (10) and (f) Cu–Mo_xC_y (25) with a magnification of ×5000.

Cu–Mo_xC_y (5) (Fig. 2(d)), the amount of large platelet particles increased, indicating that the topotactic transformation was also involved during the carburization process. In the case of Cu–Mo_xC_y (10) as shown in Fig. 2(e), many platelet particles were observed although some agglomerated isotropic particles coexisted, indicating that the topotactic transformation process became the main process during the carburization process. However, when Cu/Mo initial molar ratio was increased to 25/75, as shown in Fig. 2(f), the morphology of Cu–Mo_xC_y (25) returned back to that of pure β-Mo_2C. These SEM images were also consistent with the results of XRD analysis. As shown in Fig. 1, XRD pattern of MoO_3 revealed the enhanced peak intensities of {0*k*0} planes such as (020), (040) and (060), which indicated an anisotropic platelet structure. However, the appearance of the strong (101) peak in the XRD pattern of β-Mo_2C implied that the morphology was changed by breaking the {0*k*0} planes, as confirmed by the SEM images with agglomerated isotropic particles, which were different from the morphology of original MoO_3. The XRD results also indicated that the topotactic route was involved during the carburization process when the Cu/Mo initial molar ratio was in the range from 5/95 to 25/75.

Table 1 shows BET specific surface areas of pure β-Mo_2C and Cu–Mo_xC_y with different Cu/Mo initial molar ratios. One can see that the BET specific surface area increased with the increase in the Cu loading amount until the Cu/Mo initial molar ratio reached 10/90, and then decreased with the increase in the Cu loading amount. This phenomenon seems to have strong relationship with the amount of α-MoC_{1-x} in the catalysts since

Table 1 BET surface areas of β-Mo_2C and Cu–Mo_xC_y with different Cu doping amounts

Catalysts	BET (m^2 g^{-1})	Catalysts	BET (m^2 g^{-1})
β-Mo_2C	5.8	Cu–Mo_xC_y (10)	68.5
Cu–Mo_xC_y (1.6)	32.6	Cu–Mo_xC_y (15)	36.0
Cu–Mo_xC_y (5)	42.7	Cu–Mo_xC_y (25)	13.6

the surface area of α-MoC_{1-x} is generally larger than that of β-Mo_2C.[23–25] In the present study, in order to understand this phenomenon in more details, TEM was used for the observation of particle surface. As shown in Fig. 3, it is found that carbon layer was formed on the Cu–Mo_xC_y particle when Cu/Mo initial molar ratio was increased over 15/85. For Cu–Mo_xC_y (25), the thickness of carbon layer reached approximately 11.3 nm (Fig. 3(d)). In contrast, no obvious carbon deposition was found in pure β-Mo_2C (Fig. 3(a)), Cu–Mo_xC_y (1.6) (Fig. 3(b)) and Cu–Mo_xC_y (10) (Fig. 3(d)) samples. It is possible that larger amount of Cu loading could promote the coke formation on the catalyst surface due to the catalytic dissociation of the methane over Cu particles during the carburization process. The formed coke on the catalyst surface could cover the pore in molybdenum carbide, and decrease the surface area. On the other hand, in this case, the promoting effect of the Cu on the topotactic solid transformation process could be decreased so that the formation of the meta-stable fcc α-MoC_{1-x} phase would be hindered. Furthermore, it should be noted that from the TEM images of Cu–Mo_xC_y (1.6) and Cu–Mo_xC_y (10), it is difficult to found single Cu particle. It is possible that Cu species were uniformly dispersed on the molybdenum carbide surface. Such well dispersion could enhance the metal-support interaction between Cu and carbide, which could be also benefit for its catalytic activity.

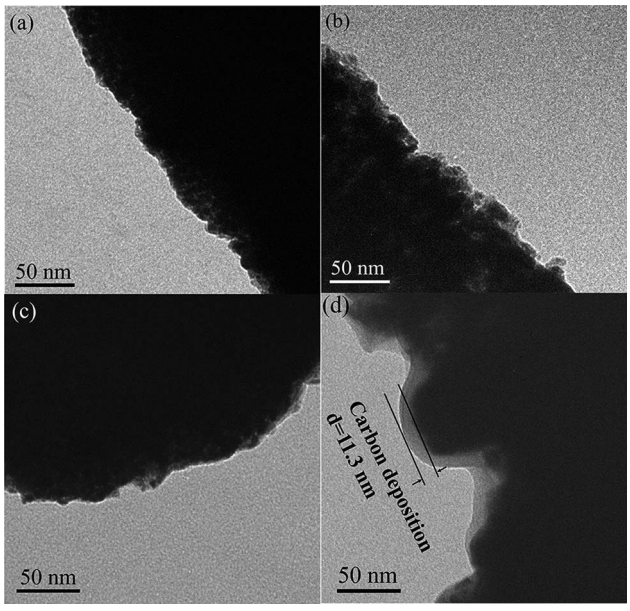

Fig. 3 Bright-field TEM morphologies of fresh as-prepared catalysts (a) β-Mo_2C; (b) Cu–Mo_xC_y (1.6); (c) Cu–Mo_xC_y (10) and (d) Cu–Mo_xC_y (25).

Effect of Cu loading amount on catalytic performance

Fig. 4 shows the effect of Cu loading amount on the catalytic performance of Cu–Mo_xC_y. One can see that the Cu loading amount had great effect on the methanol conversion in SRM reactions. When Cu/Mo initial molar ratio was lower than 10/90, the catalytic activity was increased with the increase in the Cu loading amount, and the highest methanol conversion was achieved for Cu–Mo_xC_y (10) at 300 °C. However, when Cu/Mo initial molar ratio was over 10/90, the catalytic activity decreased with the increase in the Cu loading amount, especially at the lower reaction temperatures, for Cu–Mo_xC_y (25), worse catalytic performance was shown, which is similar to that of the undoped molybdenum carbide, *i.e.* β-Mo_2C as indicated in our previous work.[6]

Such a tendency of catalytic performance of Cu–Mo_xC_y catalyst is actually in agreement with their physicochemical properties as indicated in Fig. 1–3 and Table 1. Especially, Cu–Mo_xC_y (10) had the largest specific surface area among the as-prepared catalysts. In general, higher surface area could provide more active sites and improve the dispersion of the Cu particles on the molybdenum carbide, which is beneficial for the catalytic performance. It should be noted that no peaks corresponding to Cu metal from the XRD pattern of Cu–Mo_xC_y (10) shown in Fig. 1, suggesting that Cu particles should be very small and well dispersed on the molybdenum carbide. In this study, coke formation during the carburization process was found when Cu doping amount was too high. It resulted in the worse performance of the prepared catalyst. As shown in Fig. 3(c), for the high Cu loading sample, *i.e.*, Cu–Mo_xC_y (25), since the fresh catalyst surface was covered by the coke layer, which could hinder the reactant to be adsorbed on the surface of active sites for SRM, its catalytic activity was very low. From the Table 1, one can see that even though the BET surface area of Cu–Mo_xC_y (25) was higher than β-Mo_2C, the catalytic activity of Cu–Mo_xC_y (25) was similar to that β-Mo_2C,[6] it is possible that the active sites of Cu–Mo_xC_y (25) were covered by carbon.

On the other hand, as shown in Fig. 1, for Cu–Mo_xC_y with Cu/Mo initial molar ratios from 5/95 to 25/75, both α-MoC_{1-x} and β-

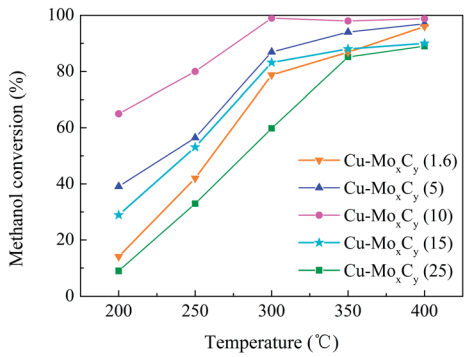

Fig. 4 Catalytic performances of Cu modified molybdenum carbide with different doping amount.

Mo_2C phases coexisted. It is reported that α-MoC_{1-x} had approximately two times higher catalytic activity than β-Mo_2C for hydrogenation of CO.[26] Hamid *et al.*[24] found that α-MoC_{1-x} showed higher methane conversion and higher stability for the non-oxidation conversion of methane to aromatic compounds when comparing with β-Mo_2C. Such performance differences in catalytic activity for the two different phases could be attributed to the differences of their surface structures: the crystal lattice of β-Mo_2C is hcp while α-MoC_{1-x} is fcc and thus more active sites could be produced on the surface of α-MoC_{1-x}. Furthermore, the local variation in the C/Mo ratio on the catalyst surface could also create different types of active sites for different reactions. For the present study, it is identified that α-MoC_{1-x} phase had much better catalytic performance for SRM than β-Mo_2C.

Fig. 5 shows the product compositions for the SRM over Cu–Mo_xC_y with Cu/Mo initial molar ratios of 1.6, 5, 10, 15 and 25, corresponding to the results shown in Fig. 4. One can see that H_2 and CO_2 were the two main components in the outlet gas, together with a small amount of CO and CH_4. In the present study, only traces of other products such as C_2H_6, C_2H_4 and HCOOH were detected for any of the catalysts. With the increase in the reaction temperature, CO concentration in the product was found to be increased while H_2 and CO_2 concentrations were decreased to some extent over any of the catalysts. It is possible that Cu doped molybdenum carbide catalysts have capability to activate water gas shift (WGS) reaction at lower temperatures (eqn (2)).[4,9]

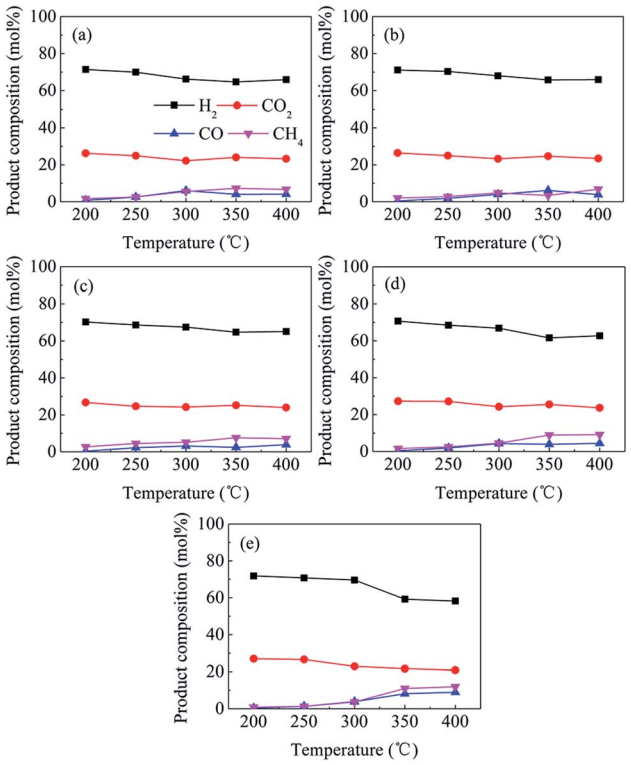

Fig. 5 Product compositions for SRM over the catalysts (a) Cu–Mo_xC_y (1.6); (b) Cu–Mo_xC_y (5); (c) Cu–Mo_xC_y (10), (d) Cu–Mo_xC_y (15) and (e) Cu–Mo_xC_y (25) corresponding to Fig. 4.

$$CO + H_2O \rightarrow CO_2 + H_2,\ \Delta H^0_{298\ K} = -41\ kJ\ mol^{-1} \quad (2)$$

This reaction is an important step to decrease the yield of CO from the steam reforming reaction for the hydrogen production. On the other hand, it should be noted that the catalysts with higher Cu loading were not benefit for the activating of WGS reaction (eqn (2)), especially at the higher reaction temperatures. Comparing with other Cu loading catalysts, H_2 concentration dropped from 70 to 57% while CO concentration increased from 0 to 10% in the reaction temperature range of 200–400 °C over the Cu–Mo_xC_y (25) catalyst. The surface of molybdenum carbide has reductive property, which is suitable for the adsorption and activation of H_2O molecule, activating the WGS reaction. The higher Cu loading could occupy more reductive surface of molybdenum carbide and prohibit the water adsorption on its active sites.

CH_4 is another unwanted by-product for the hydrogen production from SRM. In the present study, the yield of hydrogen can be considered as the result of the competition between the WGS reaction and methanation (eqn (3)).

$$CO + 3H_2 \rightarrow CH_4 + H_2O,\ \Delta H^0_{298\ K} = -206\ kJ\ mol^{-1} \quad (3)$$

Herein, it should be noted that 1 mole of methane production will result in a loss of 4 moles of hydrogen. Therefore, based on the WGS reaction (eqn (2)) and methanation reaction (eqn (3)), more hydrogen can be extracted from steam and methanol during the steam reforming process if the methanation reaction is hindered. As indicated in Fig. 5, with the increase in Cu loading amount, the methane composition in the outlet gas was increased, especially at the high reaction temperature, indicating that the methanation reaction could be effectively hindered by decreasing Cu loading amount.

Stability performances of Cu–Mo_xC_y catalysts

Long-term catalytic activity tests for pure β-Mo_2C and Cu–Mo_xC_y with Cu/Mo initial molar ratios of 1.6/98.4, 5/95, 10/90, 15/85 and 25/75 at 400 °C at first. As shown in Fig. 6, for the pure β-Mo_2C catalyst, the catalytic activity was unstable, and after 9 h,

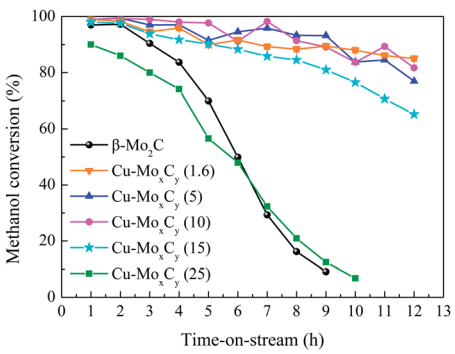

Fig. 6 Time-on-stream testing of β-Mo_2C, Cu–Mo_xC_y (1.6), Cu–Mo_xC_y (5), Cu–Mo_xC_y (10), Cu–Mo_xC_y (15) and Cu–Mo_xC_y (25) catalysts for SRM at 400 °C. (WHSV = 9000 $cm^3\ g^{-1}\ h^{-1}$ and steam-to-carbon molar ratio = 1).

the methanol conversion dropped from 100% to a value as low as 10%. However, when Cu doped on the molybdenum carbide surface with Cu/Mo initial molar ratios of only 1.6/98.4, the catalytic stability was enhanced greatly. Herein, the stability performances of Cu–Mo_xC_y (5) and Cu–Mo_xC_y (10) were almost the same as that of Cu–Mo_xC_y (1.6). When the Cu/Mo initial molar ratio was increased more, the catalytic activity begun to decrease faster, and for Cu–Mo_xC_y (25), the catalytic stability performance decreased sharply and near to that of the pure β-Mo_2C catalyst.

Fig. 7 shows product compositions during the SRM stability test related to Fig. 6. For the pure β-Mo_2C catalyst, the outlet gas compositions were also unstable. One can see that the CO percentage in outlet gas was increased from 5% to about 20% while CO_2 percentage in outlet gas decreased from 23 to 10% after 9 h reaction although the H_2 percentage was decreased a little. Here, it should be noted that the methanol conversion was sharply decreased from 100 to 10% in this case (Fig. 6). On the other hand, when β-Mo_2C surface was modified by a little amount of Cu, the stability of the product composition was enhanced obviously. As indicated in Fig. 7(a), for Cu–Mo_xC_y (1.6), the CO_2 percentage was decreased from 23 to 15%, and CO percentage increased from 2 to 14% with the time-on-stream. For Cu–Mo_xC_y (5) and Cu–Mo_xC_y (10), as shown in Fig. 7(c) and (d), respectively, the outlet gas composition stability was very high. Especially for Cu–Mo_xC_y (10), as shown Fig. 7(d), it is found that the H_2 percentage remained at approximately 60%, CO_2 percentage was slowly decreased from 23 to 20% after 12 h reaction and CO percentage was slowly increased from 2 to 8% with the time-on-steam. For Cu–Mo_xC_y (25), as shown in Fig. 7(e), although the H_2 percentage in the outlet gas was increased from 53 to 63% after 12 h reaction while the CO_2 composition was decreased from 21 to 17% after 12 h reaction, it should be noted that the methanol conversion was sharply decreased from the 100% to 9% in this case (Fig. 6).

Fig. 8 shows the XRD patterns of the spent catalysts after the long-term stability tests as indicated in Fig. 6. No evidence of MoO_3 and other molybdenum oxide formations were found. This indicated that the deactivation of the pure β-Mo_2C and Cu–Mo_xC_y (25) was not resulted from the bulk oxidation of

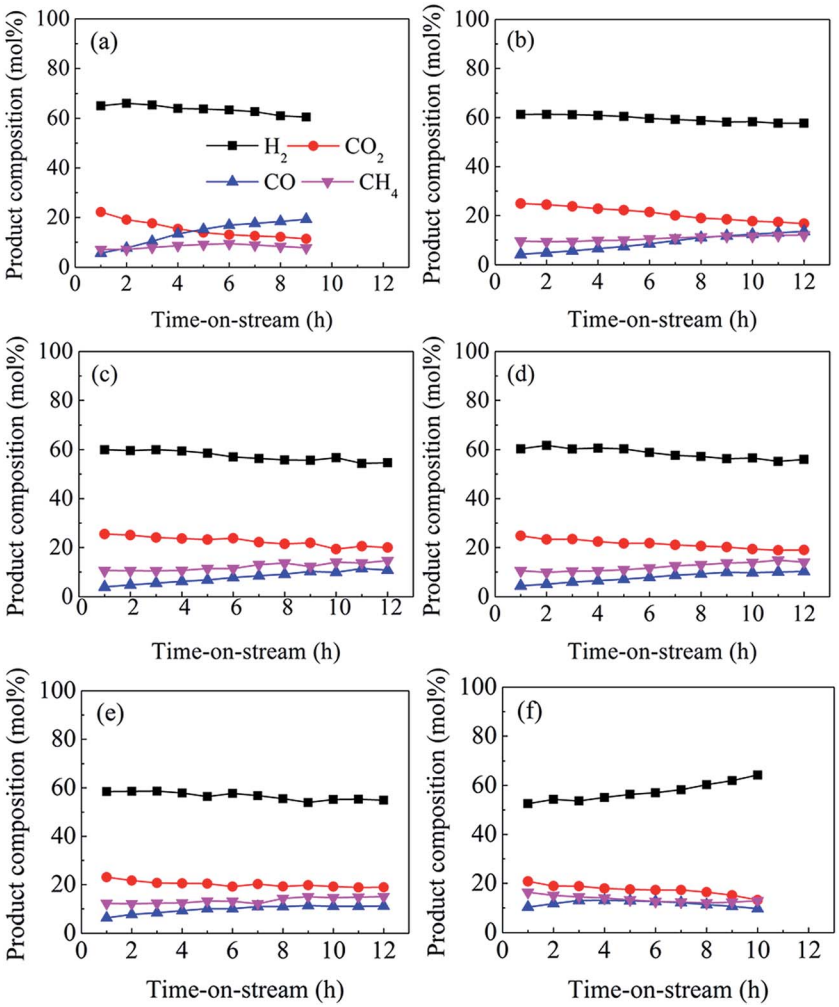

Fig. 7 Product compositions for the stability experiment of SRM over Cu–Mo_xC_y catalysts corresponding to Fig. 6. (a) β-Mo_2C; (b) Cu–Mo_xC_y (1.6); (c) Cu–Mo_xC_y (5); (d) Cu–Mo_xC_y (10), (e) Cu–Mo_xC_y (15) and Cu–Mo_xC_y (25).

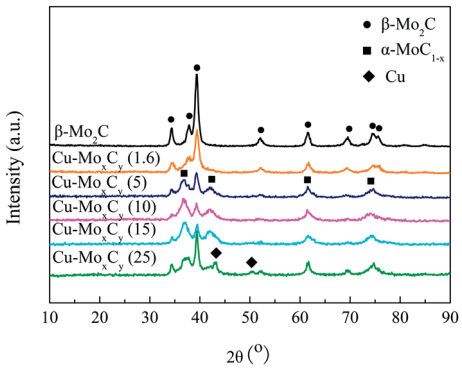

Fig. 8 XRD patterns of the spent catalysts of β-Mo_2C, Cu–Mo_xC_y (1.6), Cu–Mo_xC_y (5), Cu–Mo_xC_y (10), Cu–Mo_xC_y (15) and Cu–Mo_xC_y (25) after the long-term stability tests shown in Fig. 6.

molybdenum carbide. As reported in our previous studies,[6,15,16] the deactivation of pure β-Mo_2C could be mainly caused by the surface oxidation. Since the surface of the fresh molybdenum carbide surface is in the reduced state, H_2O molecules should be adsorbed and dissociated on it. Moon *et al.*[3] reported that the deactivation of pure β-Mo_2C during the thermal cycling run for water gas shift reaction was caused by the oxidation of carbide surface to MoO_3. However, H_2O molecules is not easily adsorbed and dissociated on the surface of MoO_3. As such, the surface oxidation of molybdenum carbide could prevent the H_2O adsorption and dissociation on its surface, resulting in the decrease of the catalytic activity. On the other hand, comparing with the XRD results shown in Fig. 1, Cu diffraction peaks were found in the spent Cu–Mo_xC_y (25) catalyst (Fig. 8). It is reported that deactivation of Cu based catalyst is generally attributed to the copper sintering.[27,28] In the present study, Cu particles could be also easily sintered on the surface of molybdenum carbide during SRM reaction in the case of high Cu loading, for instance, Cu–Mo_xC_y (25) catalyst. In contrary, as will discussed in section 3.4, a strong metal-support interaction (SMSI) due to the well dispersion of Cu resulted in more Cu^{I} species, which is benefit to stabilize Cu particles on the molybdenum carbide surface, preventing the sintering, were produced in the cases of the lower Cu loading amounts, *i.e.*, Cu–Mo_xC_y (5) and Cu–Mo_xC_y (10). Hence, only in the case of loading lower amount of Cu could enhance the stability. Furthermore, the dissociation and activation of CH_3OH could be greatly enhanced by doping of Cu on molybdenum carbide surface. Herein, Cu modified molybdenum carbide catalyst is a bi-functional catalyst, in which the H_2O molecule will be adsorbed and dissociated on molybdenum carbide surface while the CH_3OH molecular will be adsorbed and activated on the Cu particles.

As shown in Fig. 4, Cu–Mo_xC_y (10) had the highest methanol conversion at 300 °C. Here, a longer term stability test was also conducted at this temperature for it. As shown in Fig. 9(a), one can see that the catalytic activity of the Cu–Mo_xC_y (10) was very stable in 50 h test, and the methanol conversion was decreased slowly from 100 to 90% while the hydrogen production rate was almost remained at 1000 μmol g-cat^{-1} min^{-1}. On the other hand, as shown in Fig. 9(b), all outlet gas concentrations also

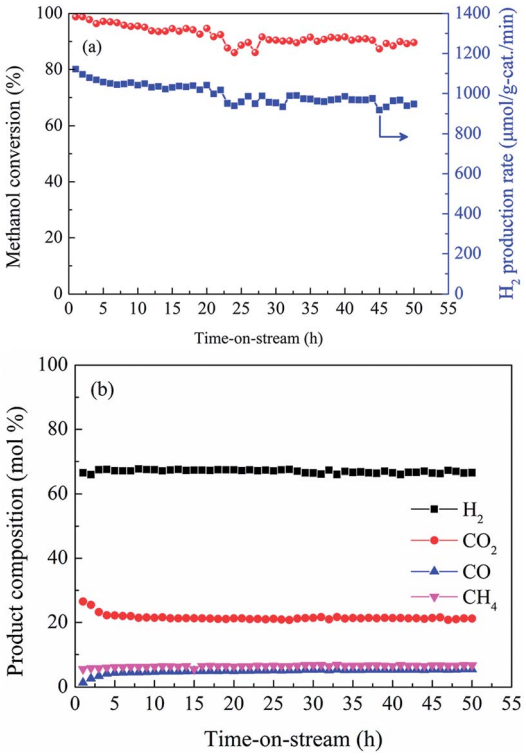

Fig. 9 Time-on-steam testing of Cu–Mo_xC_y (10) catalyst for the SRM at 300 °C for 50 h: (a) methanol conversion and H_2 production rate and (b) product composition. (WHSV = 9000 cm^3 g^{-1} h^{-1} and steam-to-carbon molar ratio = 1).

remained very stable in 50 h test, and the H_2 concentration in the product stream was kept at *ca.* 68% while CO_2, CH_4, and CO concentrations were kept at *ca.* 20%, 6%, and 6%, respectively, in the outlet gas product stream, indicating that Cu–Mo_xC_y (10) had excellent activity stability for the SRM at relativity low reaction temperature. In our previous study,[16] Ni modified molybdenum carbide catalyst was applied for SRM reaction for hydrogen production, and Ni–Mo_2C (2.4) also showed high activity and stability at a reaction temperature of 300 °C. However, in the present study, Cu modified molybdenum carbide (Cu–Mo_xC_y (10)) showed higher stability than Ni–Mo_2C (2.4), indicating that Cu modified molybdenum carbide catalyst (Cu–Mo_xC_y (10)) should be more suitable for *in situ* production of hydrogen from SRM.

XPS analysis of Cu–Mo_xC_y catalysts

Fig. 10 shows Cu 2p peaks obtained from XPS analysis of the fresh Cu–Mo_xC_y with Cu/Mo initial molar ratios of 5/95, 10/90 and 25/75. Cu 2p transition generally appears at the binding energy value lower than 933 eV for metallic copper (Cu) and Cu^{I}, and the binding energy value appeared at the value higher than 933 eV is attributed to Cu^{II}.[29] The presence of Cu^{II} species on the fresh catalyst can be also identified from the intense satellite peak at a binding energy of 940–945 eV in the XPS spectra. The presence of the satellite peak is due to the interaction of the ejected photoelectron with the other valence band electron, and

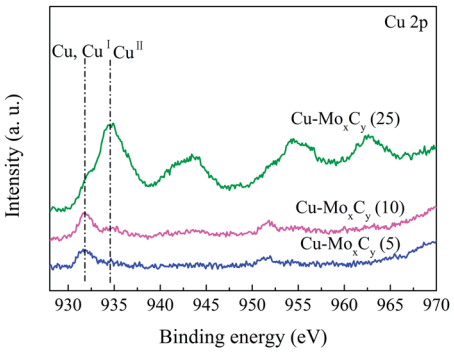

Fig. 10 XPS spectra of Cu 2p of as-prepared Cu–Mo$_x$C$_y$ catalysts with different copper loading amounts.

the metal to ligand charge transfer could occur in Cu^{II} species. However, the satellite peaks are generally not presented in Cu and Cu^{I} species due to their full 3d band. In the present study, as shown in Fig. 10, with the increase in the Cu loading amount, Cu 2p banding energy was shifted from 931.7 to 934.3 eV, indicating that the copper species on the molybdenum carbide were changed from the Cu and Cu^{I} species to Cu^{II} species. Especially for the Cu–Mo$_x$C$_y$ (25) sample, the major copper species on the surface was Cu^{II} species. It indicated Cu particles might be agglomerated and the interaction between the metal and support became weak since the loading amount was too high. In contrast, in the range of Cu/Mo initial molar ratio between 5/95 and 10/90, with the increase in the Cu loading amount, the amount of Cu and Cu^{I} species on the catalysts surface was also increased.

Although Cu 2p XPS results shown in Fig. 10 indicated that the metal Cu and/or Cu^{I} species existed in the Cu–Mo$_x$C$_y$ catalysts, it is difficult to differentiate between the metal Cu and Cu^{I} valence states since electronic binding energies could be only separated by a small fraction of potential due to the relatively large Cu radius.[30] As such, in order to determine the valence states of various Cu species, the kinetic energy of the ejected Auger electron was tested. The Cu Auger kinetic energy regions obtained from the fresh Cu–Mo$_x$C$_y$ catalysts are shown in Fig. 11. The Cu LMM Auger kinetic peaks centered at about 915 eV and 918 eV, which attributed to Cu^{I} and Cu metal,[30–32] were observed, respectively. From the Fig. 11, one can see that Cu^{I} should be the main species on Cu–Mo$_x$C$_y$ (5) and Cu–Mo$_x$C$_y$ (10) surfaces. Considering the asymmetry peak of the spectra of Cu–Mo$_x$C$_y$ (5) and Cu–Mo$_x$C$_y$ (10), it is possible that small amount of Cu metal was also coexisted on the surface. Considering the catalytic activity shown in Fig. 4, it can be speculated that Cu^{I} played an important role for the improvement of molybdenum carbide activity.

In the present study, the co-existence of Cu^{I} and Cu^{II} species might be due to the passivation treatment of the fresh catalysts using 1% O_2/Ar. In the case of lower Cu loading, *i.e.*, Cu–Mo$_x$C$_y$ (5) and Cu–Mo$_x$C$_y$ (10), the Cu particles could be better dispersed on the molybdenum carbide surface, and the interaction between Cu and Mo$_x$C$_y$ would prevent the oxidation of Cu. In the catalyst, the Cu particles could be surrounded by

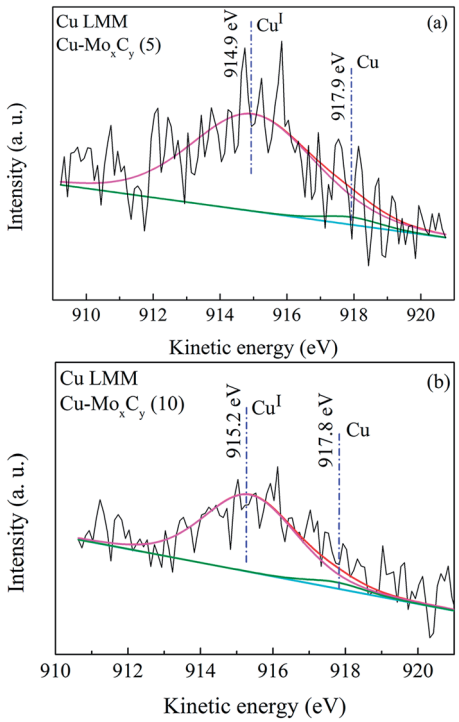

Fig. 11 Auger Cu LMM spectra of as-prepared Cu–Mo$_x$C$_y$ catalysts with different copper loading amounts. (a): Cu–Mo$_x$C$_y$ (5); (b): Cu–Mo$_x$C$_y$ (10).

molybdenum carbide, forming a structure like Cu–O–C or Cu–O–Mo, in which Cu can just be partially oxidized by O, resulting in the appearance of Cu^{I} species. In contrast, in the case of higher Cu loading, *i.e.*, Cu–Mo$_x$C$_y$ (25), the Cu particles could be agglomerated on the surface of molybdenum carbide at high carburization temperature (700 °C) and thus, the interaction between Cu and molybdenum carbide support becomes weak

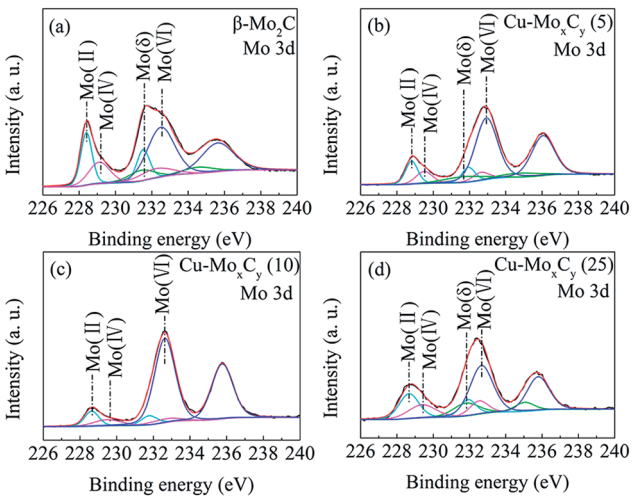

Fig. 12 XPS spectra of Mo 3d of (a) fresh β-Mo$_2$C and (b) Cu–Mo$_x$C$_y$ (5), (c) Cu–Mo$_x$C$_y$ (10) and (d) Cu–Mo$_x$C$_y$ (25).

Table 2 Mo $3d_{5/2}$ binding energy of the fresh β-Mo_2C and Cu–Mo_xC_y (Cu/Mo initial molar ratios = 5/95, 10/90, 25/75) catalysts

	Mo $3d_{5/2}$ (eV)			
Catalysts	Mo^{II} (Mo_2C)	Mo^{IV} (MoO_2)	Mo^{δ} (MoO_xC_y)	Mo^{VI} (MoO_3)
β-Mo_2C	228.4	229.1	231.4	232.5
Cu–Mo_xC_y (5)	228.7	229.3	231.7	232.9
Cu–Mo_xC_y (10)	228.8	230.5	—	232.7
Cu–Mo_xC_y (25)	228.7	229.4	231.9	232.6

so that Cu metal was easily oxidized by the passivation gas of 1% O_2/Ar.

For further investigation of the interaction between Cu and molybdenum carbide support. Mo 3d XPS analysis was also carried out to elucidate the chemical states of molybdenum carbide support. The Mo 3d peaks obtained from the fresh β-Mo_2C and Cu–Mo_xC_y (Cu/Mo initial molar ratios: 5/95, 10/90, 25/75) catalysts are shown in Fig. 12, and the binding energy of the corresponding Mo 3d XPS peaks is summarized in Table 2. Herein, the double peaks should have a splitting of ~3.13 eV and a Mo $3d_{5/2}$ to $3d_{3/2}$ ratio of 3 : 2, and the distribution of Mo state was estimated by means of deconvolution. It is found that there were four molybdenum species on pure molybdenum carbide surface: the one with $3d_{5/2}$ binding energy (BE) of 228.4 eV was attributed to Mo^{II} species involved in Mo–C bonding, and other three with $3d_{5/2}$ binding energies of 229.1, 231.4 and 232.5 eV were identified as Mo^{IV}, Mo^{δ} (where δ is the states between IV and VI) and Mo^{VI}, respectively. Mo^{IV}, Mo^{δ} and Mo^{VI} species involved in Mo–O and Mo–O–C bonding. No peak corresponding to metallic Mo was detected. The existence of molybdenum oxide should be attributed to the surface oxide formed during passivation process.[5] However, the possibility that some oxides were produced from the incomplete carburization could not be denied although these oxides were not detected from XRD analysis since its particle size was too small with a minor amount on the catalyst surface.

Similar Mo 3d XPS spectra were observed for Cu doped molybdenum carbide (Fig. 12(b–d)). However, it should be noted that the Mo^{δ} species were not detected in the Cu–Mo_xC_y (10) sample. XPS analysis helped to disclose the features of copper interaction with the molybdenum carbide surface. From the binding energy results summarized in Table 2, one can see that copper addition caused a change in the electronic band structure of Mo^{II} species. The binding energy of Mo^{II} species shifted to the higher binding energy when Cu was doped on the molybdenum carbide surface. Here, the binding energy shift of Mo^{II} species is the indicative of charge transfer from the matrix to the Cu metal, indicating a strong interaction between the Cu and molybdenum carbide.

All these XPS analysis results indicated that a strong metal support interaction (SMSI) existed in Cu doped molybdenum carbide and the interaction strength was strongly correlated with the Cu loading amount. Schweitzer *et al.*[2] reported that the strong interaction between Pt and molybdenum carbide should be existed when Pt was doped on the unpassivated β-Mo_2C surface. They believed that this was the main reason why the obtained Pt-doped molybdenum carbide had very high catalytic activity for WGS reaction. In the present study, the existence of Cu^{I} species on the surface of Cu–Mo_xC_y catalyst was considered as one of the main reasons why the obtained catalysts such as Cu–Mo_xC_y (10) had very high catalytic activity for SRM. Therefore, it can be speculated that the real active site was located on the Cu particle perimeter between support and metal surface as shown in Fig. 13. Furthermore, based on the Mo 3d XPS results, the formation of Cu^{I} species should be also due to the strong metal-support interaction (SMSI) in the catalysts.

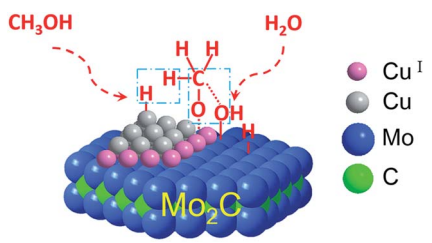

Fig. 13 Schematic structure of Cu modified molybdenum carbide catalyst with low Cu loading amount.

Conclusions

Cu modified molybdenum carbide (Cu–Mo_xC_y) catalysts were prepared by carburization of Cu doped molybdenum oxide (Cu–MoO_3) using temperature-programmed reaction with a 20% CH_4–H_2 mixture at 700 °C and used for SRM at a temperature in the range of 200–400 °C. The following results were obtained:

(1) Phase transition of the molybdenum carbide was found to be related to the doping amount of Cu: with the increase in Cu doping amount from Cu/Mo molar ratio of 1.6/98.4 to 10/90, cubic α-MoC_{1-x} phase increased in the catalyst, but with the continuous increase of Cu doping amount to a Cu/Mo molar ratio of 15/85, the α-MoC_{1-x} phase began to decrease, and when the Cu/Mo molar ratio reached to 25/75, the α-MoC_{1-x} phase almost disappeared and mainly hexagonal β-Mo_2C phase was found in the catalyst.

(2) TEM images indicated that the formation of carbon on Mo_xC_y surface occurred during the carburization process in the case of high Cu doping. It indicated that Cu had catalytic activity to decompose of methane during the carburization process and resulted in the formation of carbon on Mo_xC_y.

(3) Cu doping amount had great effect on the catalytic activity for SRM reactions. Cu–Mo_xC_y catalyst with a Cu/Mo

molar ratio of 10/90 was found to have the highest catalytic activity as well as the long-term stability at a reaction temperature of 300 °C.

(4) X-ray photoelectron spectroscopy analysis indicated that the coexistence of Cu^{I} and Cu^{II} species on the surface of the Cu doped molybdenum carbide. The existent of Cu^{I} could result in high activity for methanol conversion and high stability of the catalyst, which might be produced due to the strong interaction between Cu and Mo_xC_y support.

Acknowledgements

This work is supported by Japan Science and Technology Agency (JST), Japan and Aomori City Government. Ma thanks the State Scholarship Fund of China Scholarship Council (2012). The authors also thank Dr Yutaka Kasai and Dr Seiji Kakuta at Aomori Prefectural Industrial Technology Research Center for their technical support on experiments.

Notes and references

1 L. Volpe and M. Boudart, *J. Phys. Chem.*, 1986, **90**, 4874.
2 N. M. Schweitzer, J. A. Schaidle, O. K. Ezekoye, X. Pan, S. Linic and L. T. Thompson, *J. Am. Chem. Soc.*, 2011, **133**, 2378.
3 D. J. Moon and J. W. Ryu, *Catal. Lett.*, 2004, **92**, 17.
4 J. Patt, D. J. Moon, C. Phillips and L. Thompson, *Catal. Lett.*, 2000, **65**, 193.
5 C. Shi, A. Zhang, X. Li, S. Zhang, A. Zhu, Y. Ma and C. Au, *Appl. Catal., A*, 2012, **431**, 164.
6 Y. Ma, G. Guan, C. Shi, A. Zhu, X. Hao, Z. Wang, K. Kusakabe and A. Abudula, *Int. J. Hydrogen Energy*, 2014, **39**, 258.
7 R. Barthos and F. Solymosi, *J. Catal.*, 2007, **249**, 289.
8 W. Setthapun, S. K. Bej and L. T. Thompson, *Top. Catal.*, 2000, **49**, 73.
9 Á. Koós, R. Barthos and F. Solymosi, *J. Phys. Chem. C*, 2008, **112**, 2607.
10 S. Li, W. B. Kim and J. S. Lee, *Chem. Mater.*, 1998, **10**, 1853.
11 L. Volpe and M. Boudart, *J. Solid State Chem.*, 1985, **59**, 332.
12 J. S. Lee, L. Volpe, F. H. Ribeiro and M. Boudart, *J. Catal.*, 1988, **112**, 44.
13 A. Széchenyi and F. Solymosi, *J. Phys. Chem. C*, 2007, **111**, 9509.
14 K. T. Jung, W. B. Kim, C. H. Rhee and J. S. Lee, *Chem. Mater.*, 2004, **16**, 307.
15 Y. F. Ma, G. Q. Guan, C. Shi, A. Zhu, X. Hao, Y. Kasai and A. Abudula, *Innovative Materials for Processes in Energy Systems*, ed. B. B. Saha, M. Koyama and Y. Takata, Research Publishing Services, 2013, pp. 45–46.
16 Y. Ma, G. Guan, P. Phanthong, X. Hao, W. Huang, A. Tsutsumi, K. Kusakabe and A. Abudula, *J. Phys. Chem. C*, 2014, **118**, 9485.
17 C. Y. Wang, M. Boucher, M. Yang, H. Saltsburg and M. Flytzani-Stephanopoulos, *Appl. Catal., B*, 2014, **154**, 142.
18 Y. H. Chin, R. Dagle, J. Hu, A. C. Dohnalkova and Y. Wang, *Catal. Today*, 2002, **77**, 79.
19 P. Yaseneva, S. Pavlova, V. Sadykov, E. Moroz, E. Burgina, L. Dovlitova, V. Rogov, S. Badmaev, S. Belochapkin and J. Ross, *Catal. Today*, 2008, **138**, 175.
20 Y. Matsumura and H. Ishibe, *J. Mol. Catal. A: Chem.*, 2011, **345**, 44.
21 C. Fukuhara, Y. Kamata and A. Igarashi, *Appl. Catal., A*, 2007, **330**, 108.
22 C. Pojanavaraphan, A. Luengnaruemitchai and E. Gulari, *Int. J. Hydrogen Energy*, 2013, **38**, 1348.
23 R. Kojima and K. Aika, *Appl. Catal., A*, 2001, **219**, 141.
24 C. Bouchy, I. Schmidt, J. Anderson, C. Jacobsen, E. Derouane and S. Derouane-Abd Hamid, *J. Mol. Catal. A: Chem.*, 2000, **163**, 283.
25 M. Tsuji, T. Miyao and S. Naito, *Catal. Lett.*, 2000, **69**, 195.
26 G. Ranhotra, A. Bell and J. Reimer, *J. Catal.*, 1987, **108**, 40.
27 S. Sá, H. Silva, L. Brandão, J. M. Sousa and A. Mendes, *Appl. Catal., B*, 2010, **99**, 43.
28 V. Durga Kumari, M. Subrahmanyam, A. Ratnamala, D. Venugopal, B. Srinivas, M. Phanikrishna Sharma, S. Madhavendra, B. Bikshapathi, K. Venkateswarlu and T. Krishnudu, *Catal. Commun.*, 2002, **3**, 417.
29 M. C. Biesinger, L. W. Lau, A. R. Gerson and R. S. C. Smart, *Appl. Surf. Sci.*, 2010, **257**, 887.
30 A. Yin, X. Guo, W. L. Dai and K. Fan, *J. Phys. Chem. C*, 2009, **113**, 11003.
31 L. Chen, P. Guo, M. Qiao, S. Yan, H. Li, W. Shen, H. Xu and K. Fan, *J. Catal.*, 2008, **257**, 172.
32 H. Lin, X. Zheng, Z. He, J. Zheng, X. Duan and Y. Yuan, *Appl. Catal., A*, 2012, **445**, 287.

